Uncooled Doped-Si Thermopiles for Thermal Land Imaging Applications

Emily M. Barrentine[a], Ari D. Brown[a], Carl Kotecki[a], Vilem Mikula[a,b], Riley A. Reid[c], Sang Yoon[a,d], and Alicia T. Joseph[a]

[a]NASA Goddard Space Flight Center, Greenbelt, MD, USA
[b]American University, Washington, DC, USA
[c]North Carolina State University, Raleigh, NC, USA
[d]Science Systems And Applications Inc., Lanham, MD, USA

ABSTRACT

Sustained and enhanced land imaging is crucial for providing high-quality science data on change in land use, forest health, environment, and climate. Future thermal land imaging instruments operating in the 10-12 micron band will provide essential information for furthering our hydrologic understanding at scales of human influence, and producing field-scale moisture information through accurate retrievals of evapotranspiration (ET). To address the need for cost-effective future thermal land imaging missions we are developing novel uncooled doped-silicon thermopile detectors, an extension of a detector design concept originally developed at NASA-Goddard for planetary science applications. These doped-Si thermopile detectors have the potential to offer superior performance in terms of sensitivity, speed, and customization, when compared to current commercial-off-the-shelf uncooled detector technologies. Because cryocooler technology does not need to be fielded on the instrument, these and other uncooled detectors offer the benefit of greatly reduced instrument cost, mass, and power at the expense of some acceptable loss in detector sensitivity. We present the motivation for an uncooled thermal imaging instrument, our doped-Si thermopile detector concept, and performance expectations and comparisons. We also provide an update on the current status of this detector technology development.

Keywords: thermopiles, infrared detectors, thermal detectors, silicon

1. INTRODUCTION

Across the U.S. and globally there are ever increasing and competing demands for freshwater resources for use in agricultural production, ecosystems services and urban development. Recent studies using the Gravity Recovery and Climate Experiment (GRACE) satellite have identified severely stressed global aquifers which are being unsustainably depleted due to over-extraction, primarily in support of irrigated agriculture.[1] Extended droughts in the western and southeastern U.S. over the past decade have also exacerbated water limitations in stressed basins, provoking water wars between neighboring states.[2] To facilitate wise water management, and to develop sustainable agricultural systems that will feed the Earth's growing population into the future, there is a critical need for robust assessments of water use and of evapotranspiration (ET) at the scale of anthropogenic activity.

Water lost to the atmosphere through ET (primarily through soil evaporation and vegetation canopy transpiration in agricultural systems) serves to cool the Earth's surface. Thus measurements of the Land Surface Temperature (LST) derived from remote-sensing data in the thermal infrared band at ∼10-12 microns provides critical science information about the ET process and water use. The ability to map ET and moisture availability via satellite has broad applications: in monitoring drought and consumptive water use, administering irrigation projects, predicting local and regional water demand, and providing important boundary conditions to hydrological and weather forecast models. Given current trends in population growth and climate, accurate monitoring of the Earth's freshwater resources at field to global scales is increasingly critical.

Further author information:
E.M.B.: E-mail: emily.m.barrentine@nasa.gov, Telephone: 1 301 286 9501

NASA and the U.S. Geological Survey's next thermal land imaging instrument, the Thermal Infrared Sensor-2 (TIRS-2) instrument on Landsat-9,[3] is scheduled to launch in 2020 and will feature GaAs Quantum Well Infrared Photodetectors (QWIPs) arrays,[4] the same detector technology used on the Thermal Infrared Sensor (TIRS) instrument on Landsat-8.[5,6] Like TIRS, the TIRS-2 telescope will operate at a ∼180 K temperature in order to reduce thermal background loading, achieved by passive radiative cooling of the instrument. However, to achieve their performance, the QWIPs detector arrays are further cooled to ∼40 K using a complex 2-stage cryocooler, and a second passive radiator is required to dissipate the heat generated by this cryocooler.

In considering the future direction of detector technology for thermal land imaging, an opportunity exists for high-performance *uncooled* detector technology that could provide a more cost-effective instrument design by not requiring cryocooling. Uncooled detectors open up the possibility of future thermal land imaging instruments to be fielded on board low-cost platforms, for example, CubeSats. In addition, they could allow future thermal land imaging instruments to capitalize on the greater number of launch opportunities, such as those available under the Evolved Expendable Launch Vehicles (EELV) program. With this motivation in mind, we are developing novel uncooled thermopile detectors based on doped-Si material. We present here a high-level overview of our doped-Si thermopile detector design concept for these applications, and compare the potential performance of this technology with the TIRS thermal land imaging instrument requirements and other commercial or space-flight uncooled detector technologies. We also report on the current status of this detector technology development at NASA-Goddard.

2. DOPED-SI THERMOPILE DESIGN CONCEPT

A thermopile is a detector that uses the thermoelectric Seebeck effect, in which a voltage difference, ΔV arises across a material in response to a temperature difference, ΔT.[7] In a thermopile, incoming radiant power is absorbed in the form of heat in a thermally-isolated absorbing region. Thermal isolation structures, which consist of p- or n- type metallic or semi-conductor materials in series, respond to the incoming radiant power and the resulting temperature differential with a voltage output. For a given material and operating temperature the material's intrinsic voltage response can be quantified by a Seebeck coefficient, α [V/K], where $\Delta V = \alpha \Delta T$. Thermopile detectors are passive detectors, with no bias power required for read out and no cryogenics required for cooling.

The response of an individual thermopile detector to optical power at zero frequency is defined as the detector's optical responsivity $S = \eta n(\alpha_n + \alpha_p)/G$ [V/W]. Here η is the optical efficiency of the absorber, α_n and α_p are the Seebeck coefficients of the n- or p-type legs respectively, and n is the number of thermocouples in the detector. A thermocouple consists of one n-type and one p-type junction in series across the thermally isolated absorber region. G is the total thermal conductance of the thermal path from the hot thermally-isolated absorber region to a colder heat sink. Contributions to this thermal conductance include the conductance along the isolation structures, and via radiation and exchange gas, which also carry away heat. The conductance via exchange gas is minimal if the detectors are operated in vacuum. Like other thermal detectors, the response time of the thermopile to an optical signal is limited by the thermal time constant of the detector system $\tau = C/G$ where C is the total heat capacity of the absorber, membrane and parasitic contributions from the thermal isolation legs. The detector sensitivity can also be characterized by a specific detectivity, $D^* = \sqrt{A\Delta f}/NEP$ [cm $\sqrt{Hz}$/W], where A is the absorbing area, Δf is the electrical bandwidth and NEP is the Noise Equivalent Power [W/$\sqrt{Hz}$]. For typical thermopile designs, the detector noise is dominated by the Johnson voltage noise across the resistive thermoelectric isolation structures, $NEP_{Johnson} = \sqrt{k_B RT}/S$, where k_B is the Boltzmann constant, R is the total resistance in the electrical path across all the thermocouple junctions and T is the operating temperature. Sub-dominant contributions to noise arise due to thermal fluctuation noise across the thermal isolation path and photon noise due to statistical fluctuations in the arrival rate of photons at the absorber. D^* or NEP and the detector speed, limited by τ, are both important performance parameters to consider for thermal land imaging applications. For thermopiles, like other thermal detectors, here there is a fundamental design trade off for a given design. Reducing G, and therefore reducing NEP and increasing D^*, comes at the expense of slowing the detector's thermal time constant. Note that detector array sensitivity can also be quantified in terms of a noise-equivalent temperature differential, NETD, where the NETD depends not just on the detector and readout

performance and parameters, but also on the optical system and the temperature and emissivity of the blackbody source being observed.

To date, all of the thermopile detectors and detector arrays flown on space missions have been Bi-Sb/Bi-Te or Bi-Sb based (see Table 1). We are motivated to use doped-Si structures in our thermopile design because the material's Seebeck coefficient can be engineered to be more than an order of magnitude higher than these more commonly used Bi-Sb or Bi-Te materials.[7] Si also has the advantage of being an exceedingly strong, lightweight, and thermally robust material. Silicon is also compatible with standard semiconductor processing techniques, allowing for greater customization possibilities, and accommodation of a variety of absorber designs. Our doped-Si thermopile detector design is based on a design concept originally developed for planetary science applications at NASA-Goddard[8] and also builds on other previous efforts to develop Si thermopile detectors.[9–13]

2.1 Thermoelectric Design Considerations & Material Properties

An important aspect of thermopile detector design is optimizing the properties of the thermoelectrically sensitive material, which are functions of both the n- and p-type dopant concentrations, the isolation structure geometry, and the operating temperature. The well-known metric for optimizing a material for use in specific thermopile designs is the thermoelectric figure of merit, $Z = \alpha^2/\rho\kappa$.[7] Here α is the previously defined Seebeck coefficient, ρ is the electrical resistivity, and κ is the thermal conductivity of the p- or n-type thermoelectric material. A material with maximum Z will result in maximum thermopile signal-to-noise for a given design approach. It should be noted that the values of α, ρ, and κ in doped-Si arise from a combination of physical effects within and between the charge-carrier and phonon systems, and are not independent.

As can be seen from the thermoelectric figure of merit, a material with low thermal conductivity provides optimal detector signal-to-noise. Until more recently, the relatively high thermal conductivity of Si has been one limitation to the implementation of this material in high-performance thermoelectric detectors and devices. However, advances in Si microfabrication and micromachining techniques mean that this is no longer the case. In our thermopile design (see Figure 1), the absorbing membrane region and thermal isolation legs consist of $\leq$1 micron thick single-crystal Si, with the thermal isolation legs consisting of p-type and n-type Si. These membrane and thermal isolations legs are fabricated from the device layer of a Silicon-on-Insulator (SOI) wafer. A large decrease in the thermal conductivity is observed in this thickness regime due primarily to phonon-boundary scattering effects.[14,15] It is also possible to integrate nano-scale perforations into these Si structures, which has been shown to further reduce thermal conductivity by more than an order of magnitude.[16]

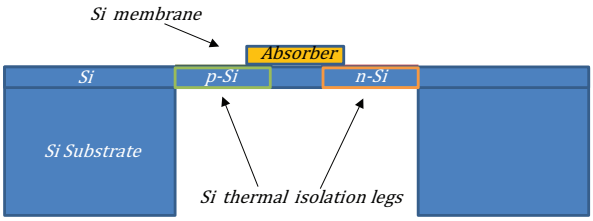

Figure 1. Cartoon cross-section of our doped-Si thermopile design which features a Si membrane with absorber and thermal isolation legs of n- or p-type, which thermally isolate the membrane from the silicon substrate.

If we do consider the thermoelectric figure of merit independent of thermal conductivity it is reduced to $Z_{reduced} = \alpha^2/\rho$. Insofar as the thermal conductivity of the material is dominated by phonon-properties and the Seebeck response of the charge-carriers can be separated from phonon effects (i.e neglecting the phonon-drag effect[23]), it is useful to examine this reduced figure of merit for Si as a function of dopant concentration and operating temperature. An example of this is shown in Figure 2 where this reduced figure of merit is calculated from measurements of Seebeck coefficient and electrical resistivity and plotted as a function of electrical resistivity. The plot includes samples from the literature, as well as our own measurements of thin Si samples. Our samples

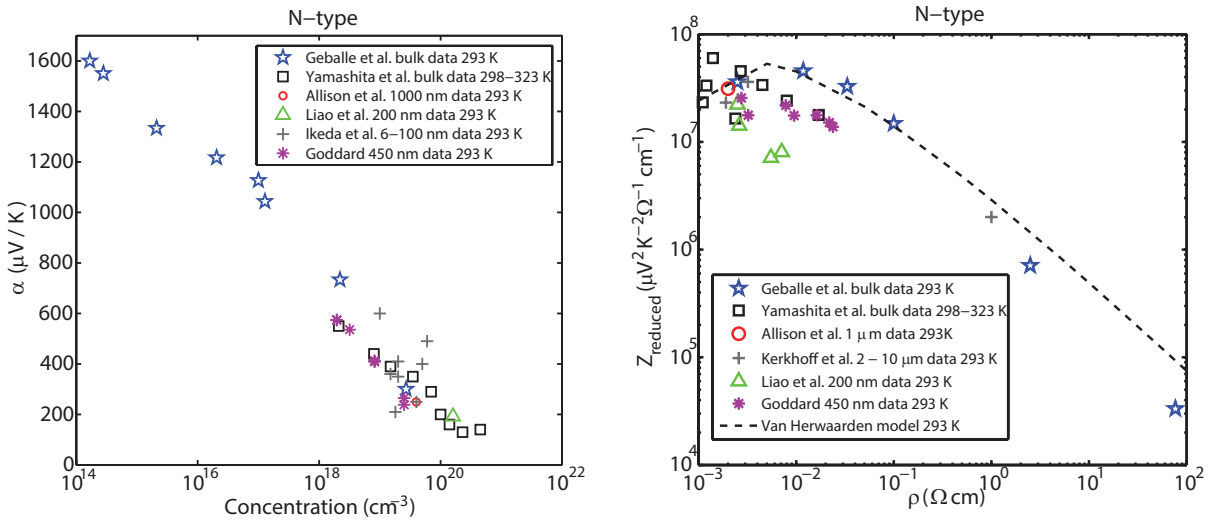

Figure 2. (Right) The measured Seebeck coefficient of p-type doped silicon as a function of dopant concentrations at room temperature. (Left) The measured p-type doped silicon reduced figure of merit, $Z_{reduced}$, as a function of electrical resistivity at room temperature. Included are measurements of bulk samples by Geballe et al. & Morin *et al.*,[17,18] bulk samples by Yamashita *et al.*,[19,20] 1 micron thick samples by Allison *et al.*,[9] 2-10 micron thick samples by Kerkhoff *et al.*,[21] 200 nm thick samples by Liao *et al.*, 6-100 nm thick samples by Ikeda *et al.*,[22] and our own 450 nm thick samples. Our measurements only indicate lower limits due to a systematic uncertainty in the interface resistance between the sample and substrate in our test setup, and we plan to carry out more robust measurements in the near future (see Sect. 4). Note that this reduced thermoelectric figure of merit only includes contributions from electrical resistivity and Seebeck effects and for proper optimization the thermal conductivity also needs to be evaluated.

consisted of 450 nm thick phosphorus-doped single crystal Si samples bonded to alumina substrates. Close to room temperature, and at relatively high dopant concentrations, the Seebeck coefficient of n- or p-type Si can be related to electrical resistivity by: $\alpha = 2.6(k_B/e)\ln(\rho/\rho_0)$ where e is the electron charge and $\rho_0 = 5 \times 10^6$ Ohms m.[13] This relation is also plotted in Figure 2. A similar evaluation of thermoelectric figure of merit can be carried out as a function operating temperature, and is shown in Figure 3 for a more limited bulk literature data set. From both of these material studies, it is seen that the maximum doped-Si thermoelectric figures of merit is achieved at moderately high dopant concentrations ($\sim 10^{17} - 10^{19}$ cm^{-3}), and that dopant concentration can also be fine-tuned for the detector operating temperature to maximize signal-to-noise. An improved reduced figure of merit occurs at ~170 K operating temperature, hinting that modest cooling of the detectors below room temperature (as is already implemented in the TIRS-2 telescope architecture via passive cooling) will also result in improved detector sensitivity.

2.2 Potential Detector Performance & Comparison

Custom designed state-of-the-art uncooled thermopiles have flown on several space flight instruments including the Mariner,[24] Voyager,[25] Cassini,[26] LRO,[27] MRO[28] and BepiColombo missions,[29] and are in consideration for future space-flight mission concepts.[30,31] They are also commercially available from several vendors.[32–36] The state-of-the-art in thermopile linear arrays has demonstrated pixel sizes ~70-500 microns, and specific detectivity D^* ~3×10^8 - 2×10^9 cm $\sqrt{Hz}$/W for respective time constants, τ ~2-300 ms (see Table 1).

Another competitive uncooled detector technology, which has developed a large commercial and defense presence, are uncooled vanadium oxide (VO_x) or amorphous Si (a-Si) microbolometer arrays. The best performance commercial uncooled microbolometer arrays, with pixel size ~25-35 microns, obtain NETD ~10-20 mK and $\tau \sim 5 - 20$ ms (see Table 2). Commericial microbolometer detectors have space-flight heritage in the THEMIS,[40] BepiColumbo,[41,42] SAC-D/Aquarius[43] and Akatsuki[44,45] missions. Microbolometer detector technology is also planned, or in consideration, for deployment in multiple future space-flight missions.[46–49] In these space-flight

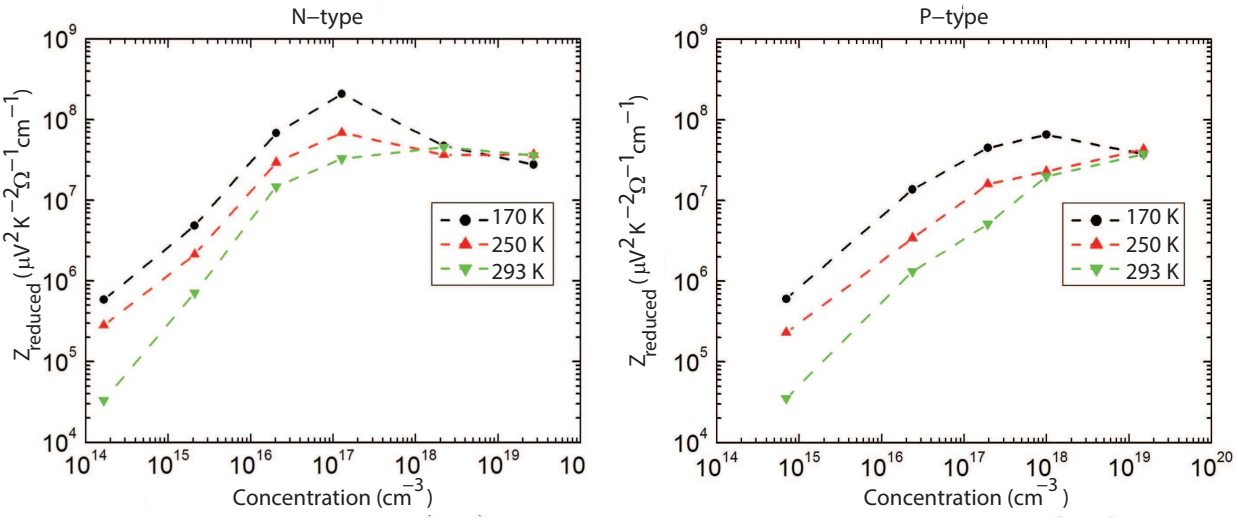

Figure 3. Example of the optimization of Si dopant concentration to achieve maximum thermoelectric performance based on bulk Si measurements by Geballe *et al.* & Morin *et al.*[17,18] at temperatures from 170 to 300 K. Optimal concentrations of $\sim 10^{17} - 10^{18}$ cm^{-3} give maximum figure of merit in these temperature regimes. Note that this reduced thermoelectric figure of merit only includes contributions from electrical resistivity and Seebeck effects and for proper optimization the thermal conductivity also needs to be evaluated.

Table 1. Comparison of potential doped-Si array designs to the best performance commercially available thermopiles, or those with space-flight heritage. Our design has the potential to achieve improved detector performance by a factor of ∼10 in sensitivity (D^*) for a similar thermal time constant. Note that a broader comparison and discussion of the performance of the current state-of-the-art in thermopile technology can be found elsewhere in the literature, for example, Dillner *et al.*[37]

Supplier	Space Mission	Material	Pixel Size [μm]	D^* [cm $\sqrt{Hz}$/W]	τ [ms]
NASA-JPL[28,38]	LRO, MCS	BiSbTe/BiTe	70-480	3×10^8 - 1.4×10^9	2-99
IPHT[29,39]	BepiColombo	BiSb/Sb	200-450	$1.3\text{-}1.6\times10^9$	150-300
NASA-GSFC	**Future**	**Si**	**∼25**	**∼2-6×10^9**	**∼5**

cases, customization of commercial designs, as well validation in relevant environments, is often required to meet specific science and instrument requirements.

Based on measured material properties (see Section 2.1) our doped-Si thermopile design has the potential to meet or exceed the performance of these current state-of-the-art uncooled thermopiles and microbolometers (see Tables 1 and 2), while offering a robust and customizable design. In addition, although the performance of cooled detectors, such as QWIPs will always offer superior performance, our doped-Si design has the potential to nearly meet or exceed NETD requirements (see Table 3) for current thermal imaging instrument designs which employ these cooled detectors, such as TIRS.

3. PROTOTYPE DETECTOR ARRAYS

We are currently exploring doped-Si detector designs with a range of pixel sizes and thermal isolation geometries, and fabrication of prototype single-pixel and linear arrays is in progress. Figure 4 shows an optical image of a prototype 1×64 doped-Si thermopile linear array, which features a 25 micron-size pixel size, comparable to the TIRS QWIPs array pixel size. Pushbroom instruments such as TIRS, as well as scanners such as the Ocean Color Instrument (OCI), only require a single row of detector pixels. Therefore, we are currently only exploring linear array architectures. Optical characterization of these first prototype doped-Si detector pixels and linear arrays is anticipated over the next few months.

Table 2. Comparison of potential doped-Si array designs to the best performance commercially available uncooled microbolometers or those with space-flight heritage. Our design has the potential to achieve detector performance comparable to, or a factor of 2 better in sensitivity (NETD) for similar thermal time constants (τ). Here NETD assumes an 8-12 micron optical band, 30 Hz, $f/1$ optics, observing a 300 K blackbody. Note that a broader comparison and discussion of the performance of the current state-of-the-art in commercial IR microbolometer technology can be found elsewhere in the literature, for example, in A. Rogalski[50] or Skidmore *et al.*[51]

Supplier	Space Mission	Material	Pixel Size [μm]	NETD [mK]	τ [ms]
SCD[52,53]	-	VO_x	25	15	$\leq$20
INO[43,54]	SAC-D/Aquarius	VO_x	35	5-14	20-13
ULIS[42,51]	BepiColumbo	a-Si	35	11	14
NASA-GSFC	**Future**	**Si**	**$\sim$25**	**8-20**	**$\sim$5**

Table 3. Comparison of potential performance of doped-Si thermopiles to the TIRS instrument requirements. Though cooled QWIPs offer superior detector performance, the TIRS instrument is limited in sensitivity by other instrument noise sources above the QWIPs detector noise level.[4] For NETD estimates we have assumed the TIRS instrument design with a 10.5 - 11.5 micron band, 90 Hz, f/1.64 optics, observing a 300 K blackbody.

	Pixel Size [μm]	NETD [mK]	τ [ms]	Operating Temperature [K]
QWIPS[4]	25	15	$<$5	43
Doped-Si Thermopiles	**$\sim$25**	**160-420**	**$\sim$5**	**170-300**
TIRS Instrument Requirement[4]	25	330	$<$5	-

4. CONCLUSIONS & FUTURE WORK

We have presented an uncooled doped-Si thermopile detector concept for thermal land imaging applications which offers the potential to improve the performance and the ability for customization of state-of-the-art thermopile detector technology. Such uncooled detectors would reduce thermal land imaging instrument costs and open up new instrument platforms, since no complex cryocooler technology is required. We are currently fabricating prototype doped-Si detector arrays and plan to carry out optical characterization of these detectors (measuring optical responsivity, detector time constant, and noise) to confirm our detector design model. In addition, we are fabricating membrane-isolated thermoelectric diagnostic structures to more robustly measure the Seebeck effect in thin doped-Si structures as a function of dopant concentration. Further consideration of high-efficiency absorber designs and array readout schemes for these detectors is also planned.

ACKNOWLEDGMENTS

The authors gratefully acknowledge funding support for this work provided by the NASA Goddard Space Flight Center Internal Research and Development Program and by the NASA Earth Science Technology Office. The significant input and contributions from Brook Lakew and Shahid Aslam during the original development of this detector design concept, as well as support from Brendan Bramman, Steve Cagiano, Nicholas Costen and Bing Guan in the setup of the doped-Si materials characterization effort, are also gratefully acknowledged.

REFERENCES

[1] Richey, A. S., Thomas, B. F., Lo, M.-H., Reager, J. T., Famiglietti, J. S., Voss, K., Swenson, S., and Rodell, M., "Quantifying renewable groundwater stress with grace," *Water Resources Research* **51**(7), 5217–5238 (2015).

[2] Gleick, P., "Water wars? here in the us?," *The Huffington Post, New York, NY, March* **1** (2013).

[3] Hair, J. H., Reuter, D. C., Tonn, S. L., McCorkel, J., Simon, A. A., Djam, M., Alexander, D., Ballou, K., Barclay, R., Coulter, P., et al., "Landsat 9 thermal infrared sensor 2 architecture and design," in [*IGARSS 2018-2018 IEEE International Geoscience and Remote Sensing Symposium*], 8841–8844, IEEE (2018).

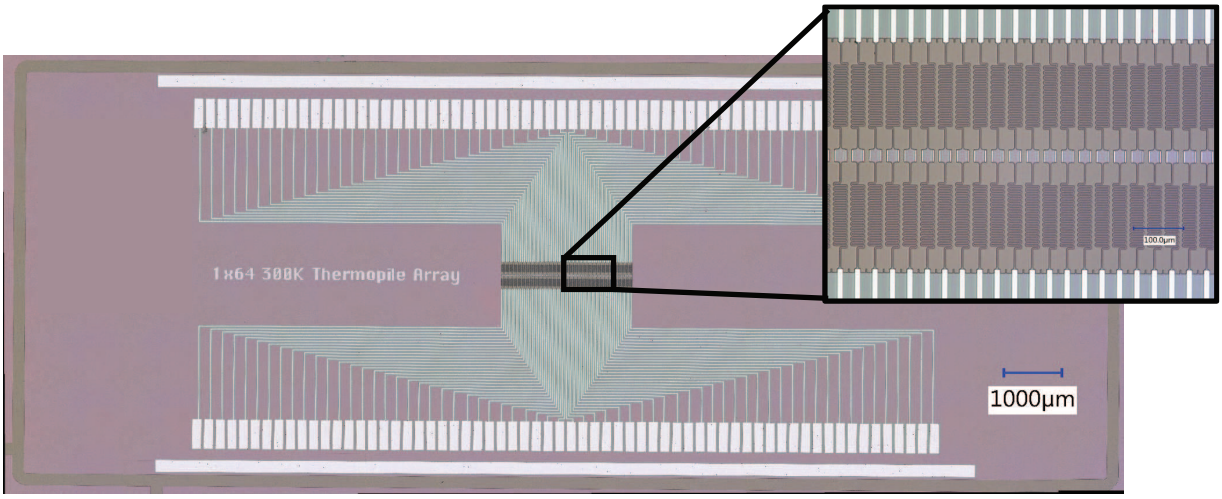

Figure 4. Optical image of a prototype 1×64 doped-Si thermopile linear array with a 25 micron pixel size.

[4] Jhabvala, M., Reuter, D., Choi, K., Jhabvala, C., and Sundaram, M., "Qwip-based thermal infrared sensor for the landsat data continuity mission," *Infrared Physics & Technology* **52**(6), 424–429 (2009).

[5] Irons, J. R., Dwyer, J. L., and Barsi, J. A., "The next landsat satellite: The landsat data continuity mission," *Remote Sensing of Environment* **122**, 11–21 (2012).

[6] Reuter, D., Richardson, C., Pellerano, F., Irons, J., Allen, R., Anderson, M., Jhabvala, M., Lunsford, A., Montanaro, M., Smith, R., et al., "The thermal infrared sensor (tirs) on landsat 8: Design overview and pre-launch characterization," *Remote Sensing* **7**(1), 1135–1153 (2015).

[7] Graf, A., Arndt, M., Sauer, M., and Gerlach, G., "Review of micromachined thermopiles for infrared detection," *Measurement Science and Technology* **18**(7), R59 (2007).

[8] Lakew, B., Barrentine, E. M., Aslam, S., and Brown, A. D., "Concept doped-silicon thermopile detectors for future planetary thermal imaging instruments," in [*AAS, Division for Planetary Sciences Meeting Abstracts*], **48** (2016).

[9] Allison, S., Smith, R., Howard, D., Gonzalez, C., and Collins, S., "A bulk micromachined silicon thermopile with high sensitivity," *Sensors and Actuators A: Physical* **104**(1), 32–39 (2003).

[10] Florin, U., Gardner, J., Ali, S. Z., Chowdhury, M. F., and Poenaru, I., "Ir detector," (2013). US Patent 8,552,380.

[11] Paige, D. F., "Microfabricated silicon thermopile sensor," (1999). US Patent 5,982,014.

[12] Nieveld, G., "Thermopiles fabricated using silicon planar technology," *Sensors and Actuators* **3**, 179–183 (1982).

[13] Van Herwaarden, A., "The seebeck effect in silicon ics," *Sensors and Actuators* **6**(4), 245–254 (1984).

[14] Liu, W. and Asheghi, M., "Phonon–boundary scattering in ultrathin single-crystal silicon layers," *Applied Physics Letters* **84**(19), 3819–3821 (2004).

[15] Asheghi, M., Kurabayashi, K., Kasnavi, R., and Goodson, K., "Thermal conduction in doped single-crystal silicon films," *Journal of Applied Physics* **91**(8), 5079–5088 (2002).

[16] Tang, J., Wang, H.-T., Lee, D. H., Fardy, M., Huo, Z., Russell, T. P., and Yang, P., "Holey silicon as an efficient thermoelectric material," *Nano letters* **10**(10), 4279–4283 (2010).

[17] Geballe, T. and Hull, G., "Seebeck effect in silicon," *Physical Review* **98**(4), 940 (1955).

[18] Morin, F. and Maita, J., "Electrical properties of silicon containing arsenic and boron," *Physical Review* **96**(1), 28 (1954).

[19] Yamashita, O. and Sadatomi, N., "Dependence of seebeck coefficient on carrier concentration in heavily b-and p-doped si1-xgex (x 0.05) system," *Japanese Journal of Applied Physics* **38**(11R), 6394 (1999).

[20] Yamashita, O., "Effect of metal electrode on seebeck coefficient of p-and n-type si thermoelectrics," *Journal of Applied Physics* **95**(1), 178–183 (2004).

[21] Kerkhoff, H. and Meyer, G., "An integrated electrothermal amplitude detector using the seebeck effect," in [*Fifth European Solid State Circuits Conference-ESSCIRC 79*], 31–33, IEEE (1979).

[22] Ikeda, H. and Salleh, F., "Influence of heavy doping on seebeck coefficient in silicon-on-insulator," *Applied Physics Letters* **96**(1), 012106 (2010).

[23] Mahan, G., Lindsay, L., and Broido, D., "The seebeck coefficient and phonon drag in silicon," *Journal of Applied Physics* **116**(24), 245102 (2014).

[24] Chase, S. C., "Infrared radiometer for the 1969 mariner mission to mars," *Applied optics* **8**(3), 639–643 (1969).

[25] Hanel, R., Crosby, D., Herath, L., Vanous, D., Collins, D., Creswick, H., Harris, C., and Rhodes, M., "Infrared spectrometer for voyager," *Applied Optics* **19**(9), 1391–1400 (1980).

[26] Kunde, V. G., Ade, P. A., Barney, R. D., Bergman, D., Bonnal, J.-F., Borelli, R., Boyd, D., Brasunas, J. C., Brown, G. V., Calcutt, S. B., et al., "Cassini infrared fourier spectroscopic investigation," in [*Cassini/Huygens: A Mission to the Saturnian Systems*], **2803**, 162–178, International Society for Optics and Photonics (1996).

[27] Paige, D., Foote, M., Greenhagen, B., Schofield, J., Calcutt, S., Vasavada, A., Preston, D., Taylor, F., Allen, C., Snook, K., et al., "The lunar reconnaissance orbiter diviner lunar radiometer experiment," *Space Science Reviews* **150**(1-4), 125–160 (2010).

[28] Foote, M., Kenyon, M., Krueger, T., McCann, T., Chacon, R., Jones, E., Dickie, M., Schofield, J., McCleese, D., and Gaalema, S., "Thermopile detector arrays for space science applications," (2004).

[29] Hänschke, F., Ihring, A., Kessler, E., Knollenberg, J., Walter, I., Dillner, U., and Meyer, H.-G., "Thermoelectric radiation sensors for the space mission bepicolombo to mercury," in [*Sensors and Systems for Space Applications VI*], **8739**, 87390E, International Society for Optics and Photonics (2013).

[30] Mariani, G., Kenyon, M., Pearson, J., and Holmes, W., "Far-infrared room-temperature focal plane modules for radiation budget instrument," in [*2016 41st International Conference on Infrared, Millimeter, and Terahertz waves (IRMMW-THz)*], 1–2, IEEE (2016).

[31] Aslam, S., Amato, M., Bowles, N., Calcutt, S., Hewagama, T., Howard, J., Howett, C., Hsieh, W.-T., Hurford, T., Hurley, J., et al., "Dual-telescope multi-channel thermal-infrared radiometer for outer planet fly-by missions," *Acta Astronautica* **128**, 628–639 (2016).

[32] "Dexter research." https://www.dexterresearch.com/.

[33] "Heimann sensor." http://www.heimannsensor.com/index.php.

[34] "Leibniz institue of photonic technology (ipht)." https://www.leibniz-ipht.de/.

[35] "Micro-hybrid electronic." https://www.micro-hybrid.de/.

[36] "Melexis." https://www.melexis.com.

[37] Dillner, U., Kessler, E., and Meyer, H.-G., "Figures of merit of thermoelectric and bolometric thermal radiation sensors," *Journal of Sensors and Sensor Systems* **2**(1), 85–94 (2013).

[38] Foote, M. C., Jones, E. W., and Caillat, T., "Uncooled thermopile infrared detector linear arrays with detectivity greater than 10^9 cm $\mathrm{hz}^{1/2}$/w," *IEEE Transactions on Electron Devices* **45**(9), 1896–1902 (1998).

[39] Dillner, U., Kessler, E., Baier, V., Berger, A., Eick, T., Behrendt, D., and Urban, H., "A 64-pixel linear thermopile array chip designed for vacuum environment," in [*Proceedings of the 9th International Conference for Infrared Sensors and Systems, Nuremberg, Germany*], **30**, 295–300 (2006).

[40] Christensen, P. R., Jakosky, B. M., Kieffer, H. H., Malin, M. C., McSween, H. Y., Nealson, K., Mehall, G. L., Silverman, S. H., Ferry, S., Caplinger, M., et al., "The thermal emission imaging system (themis) for the mars 2001 odyssey mission," *Space Science Reviews* **110**(1-2), 85–130 (2004).

[41] Benkhoff, J., Helbert, J., Team, M., et al., "Thermal infrared spectroscopy to investigate the composition of mercury–the mertis instrument on bepicolombo," *Advances in Space Research* **38**(4), 647–658 (2006).

[42] Rabaud, W., Vilain, M., Garret, T., Hopkinson, G., Bentley, M., Kraft, S., Legras, O., and Castelein, P., "Uncooled detector development for space application," in [*Sensors and Systems for Space Applications II*], **6958**, 69580P, International Society for Optics and Photonics (2008).

[43] Pope, T., Dupont, F., Blanco, S. G., Williamson, F., Chevalier, C., Marchese, L., Chateauneuf, F., Jerominek, H., Linh, N.-P., and Bouchard, R., "Space qualification of a 512x3 pixel uncooled microbolometer fpa," in [*Infrared Technology and Applications XXXV*], **7298**, 729826, International Society for Optics and Photonics (2009).

[44] Fukuhara, T., Taguchi, M., Imamura, T., Nakamura, M., Ueno, M., Suzuki, M., Iwagami, N., Sato, M., Mitsuyama, K., Hashimoto, G. L., et al., "Lir: Longwave infrared camera onboard the venus orbiter akatsuki," *Earth, Planets and Space* **63**(9), 1009–1018 (2011).

[45] Nakamura, M., Imamura, T., Ishii, N., Abe, T., Kawakatsu, Y., Hirose, C., Satoh, T., Suzuki, M., Ueno, M., Yamazaki, A., et al., "Akatsuki returns to venus," *Earth, Planets and Space* **68**(1), 75 (2016).

[46] Dartois, T., Manolis, I., Bézy, J.-L., Meynart, R., and Tisse, C.-L., "Environmental evaluation of the ulis pico1024 microbolometer," in [*Sensors, Systems, and Next-Generation Satellites XXI*], **10423**, 104231L, International Society for Optics and Photonics (2017).

[47] Fukuhara, T., Okada, T., and Tanaka, S., "New application of the uncooled microbolometer array to remote sensing for asteroids and moon," in [*Lunar and Planetary Science Conference*], **48** (2017).

[48] Adams, J., Ahmad, S., Albert, J.-N., Allard, D., Anchordoqui, L., Andreev, V., Anzalone, A., Arai, Y., Asano, K., Pernas, M. A., et al., "The infrared camera onboard jem-euso," *Experimental Astronomy* **40**(1), 61–89 (2015).

[49] Brageot, E., Groussin, O., Lamy, P., Reynaud, J.-L., Fargant, G., Licandro, J., Helbert, J., Knollenberg, J., and Kührt, E., "Thermap: A mid-infrared spectro-imager based on an uncooled micro-bolometer for space missions to small bodies of the solar system," in [*Space Telescopes and Instrumentation 2012: Optical, Infrared, and Millimeter Wave*], **8442**, 84424O, International Society for Optics and Photonics (2012).

[50] Rogalski, A., "Next decade in infrared detectors," in [*Electro-Optical and Infrared Systems: Technology and Applications XIV*], **10433**, 104330L, International Society for Optics and Photonics (2017).

[51] Skidmore, G. D., Han, C., and Li, C., "Uncooled microbolometers at drs and elsewhere through 2013," in [*Image Sensing Technologies: Materials, Devices, Systems, and Applications*], **9100**, 910003, International Society for Optics and Photonics (2014).

[52] Mizrahi, U., Schapiro, F., Bykov, L., Giladi, A., Shiloah, N., Pivnik, I., Elkind, S., Maayani, S., Mordechai, E., Farbman, O., et al., "Advanced μ-bolometer detectors for high-end applications," in [*Infrared Technology and Applications XXXVIII*], **8353**, 83531H, International Society for Optics and Photonics (2012).

[53] Mizrahi, U., Yuval, S., Hirsh, Y., Sinai, Y., Lury, Y., Gridish, Y., Syrel, N., Shamay, Y., Meshorer, R., Iosevich, R., et al., "Low-swap shutterless uncooled video core by scd," in [*Infrared Technology and Applications XLI*], **9451**, 94511E, International Society for Optics and Photonics (2015).

[54] Généreux, F., Tremblay, B., Girard, M., Paultre, J.-E., Provençal, F., Desroches, Y., Oulachgar, H., Ilias, S., and Alain, C., "On the figure of merit of uncooled bolometers fabricated at ino," in [*Infrared Technology and Applications XLII*], **9819**, 98191U, International Society for Optics and Photonics (2016).